

Harnessing β -Hydroxyl Groups in Poly(β -Amino Esters) toward Robust and Fast Reprocessing Covalent Adaptable Networks

Gyuri Lee,[#] Hyeong Yong Song,[#] Subi Choi, Chae Bin Kim, Kyu Hyun,^{*} and Suk-kyun Ahn^{*}



Cite This: *Macromolecules* 2022, 55, 10366–10376



Read Online

ACCESS |



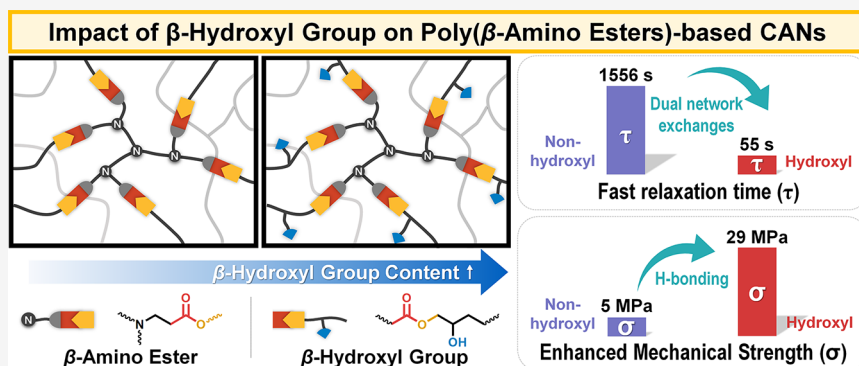
Metrics & More



Article Recommendations



Supporting Information



ABSTRACT: Poly(β -amino esters) (PBAEs), which include tertiary amines at the β -position of ester linkages, are promising in biomaterials due to their biodegradability and pH responsiveness. Such characteristics in the molecular structure are also appealing for designing catalyst-free covalent adaptable networks (CANs), but this has rarely been explored in the literature. Herein, we synthesize a series of PBAE-based CANs by aza-Michael addition, using diacrylate monomers with and without β -hydroxyl groups, and a triamine crosslinker. By leveraging hydrogen bonding, the thermal and mechanical properties of these PBAE-based CANs are effectively tuned through the monomer composition. Owing to the numerous tertiary amines serving as internal catalysts, these CANs undergo catalyst-free network exchange through a dynamic aza-Michael reaction. Interestingly, increasing the amount of β -hydroxyl groups accelerates overall stress relaxation from the synergistic effects of transesterification (associative type) at lower temperatures and dynamic aza-Michael reaction (dissociative type) at higher temperatures. Based on these features, we successfully demonstrate the reprocessing and healing at elevated temperatures under mild pressure, as well as shape memory and shape reconfiguration. Thus, controlling the β -hydroxyl group concentration in PBAE-based CANs is a useful strategy for enhancing both the mechanical strength and reprocessing rate.

INTRODUCTION

Global warming caused by carbon dioxide emission is accelerating, and the resulting climate change has motivated governments, industries, and academic researchers around the world to reduce plastic production and consumption.¹ Carbon dioxide emission may be reduced by either replacing plastics sourced from fossil fuels with sustainable materials or recycling/reusing existing plastics for multiple times. Among plastics, thermosets such as epoxies, urethanes, and rubbers have excellent mechanical properties and chemical/dimensional stability owing to their covalent network structures; and therefore, they are used in coatings, adhesives, insulations, tires, etc. Unfortunately, as their name implies, conventional thermosets cannot be reshaped but rather decompose upon heating, making their mechanical recycling extremely challenging.

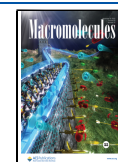
A new class of crosslinked polymers consisting of dynamic covalent bonds, called covalent adaptable networks (CANs), have gained enormous attention recently because of their

ability to undergo network rearrangement under external stimuli such as heat or light.^{2,3} Such network rearrangement leads to various useful properties (including reprocessing, welding, self-healing, and shape reconfiguration) that are impossible for conventional thermosets.⁴ In general, CANs are classified according to the mechanism of crosslink exchange into dissociative and associative CANs (Figure 1).⁵ In dissociative CANs, covalent bonds in the network first break to release network segments comprising reactive moieties. When these moieties diffuse and encounter the complementary reactive moieties, crosslinks are regenerated.⁶ Representative

Received: September 8, 2022

Revised: October 27, 2022

Published: November 28, 2022



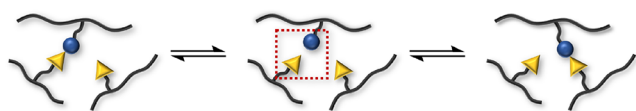
ACS Publications

© 2022 American Chemical Society

10366

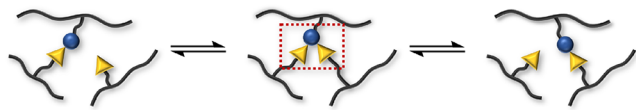
<https://doi.org/10.1021/acs.macromol.2c01872>
Macromolecules 2022, 55, 10366–10376

Dissociative CANs



ex) Diels-Alder cycloadditions, Hindered urea exchange, Boronate ester

Associative CANs



ex) Transesterification, Transcarbamylation, Transcarbonation

Figure 1. Two types of molecular network rearrangements within CANs.

examples of exchangeable chemistry in dissociative CANs include Diels–Alder cycloadditions,⁷ hindered urea exchange,⁸ oxime-enabled transcarbamylation,⁹ boronate esters,¹⁰ radical oligosulfide exchange,¹¹ thiol–Michael reaction,¹² and aza–Michael reaction.¹³ On the other hand, the associative CANs undergo simultaneous bond breakage and formation in a single step, unlike the discrete dissociation and association steps in dissociative CANs.⁶ As a result, associative CANs can maintain a constant crosslinking density during their network rearrangement. In 2011, Leibler and coworkers coined the term

“vitrimers” to describe the associative CANs by considering their unique viscosity–temperature relationship similar to that of vitreous silica.^{14–16} Transesterification^{14–16} is the most popular exchangeable reaction for associative CANs, but numerous other exchangeable chemistries have also been suggested, such as transamination of vinylogous urethanes,¹⁷ transcarbamylation,¹⁸ transcarbonation,¹⁹ imine exchange,^{20,21} olefin metathesis,^{22,23} and silyl ether exchange.²⁴

In the majority of associative CANs, network exchange often relies on external catalysts such as $\text{Zn}(\text{OAc})_2$, $\text{Zn}(\text{acac})_2$, $\text{Sn}(\text{Oct})_2$, PPh_3 , $\text{Ti}(\text{OPr})_4$, or an organic base (e.g., TBD or DBU), and their stress–relaxation kinetics can be regulated by the catalyst type and concentration.²⁵ However, the presence of low-molecular-weight catalysts in polymer networks may also cause leakage of toxic materials or thermal decomposition after repeated recycling processes.²⁶ To eliminate catalysts from CANs, researchers recently developed the concepts of internal catalysis and neighboring group participation (NGP), which often enable or accelerate network exchange by altering the electronic environment around the exchangeable bonds.^{26,27} For example, the transesterification rate can be promoted using the following approaches: (1) introducing hydroxyl groups in the β -position of ester linkages,^{14,28} (2) incorporating carboxylic or sulfonic acid groups in proximity of an ester group,²⁹ (3) harnessing the inductive effect of CF_3

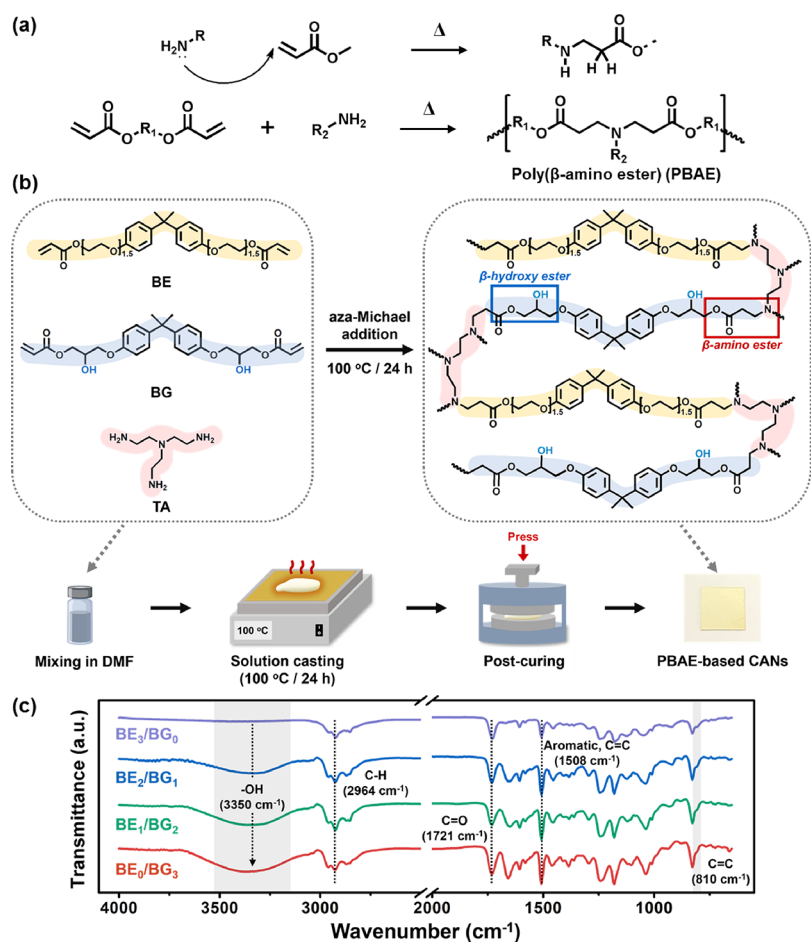


Figure 2. General reaction scheme of (a) β -amino ester (top) and poly(β -amino esters) (PBAE) (bottom) produced by aza-Michael addition reaction between a diacrylate and an amine. (b) Synthesis of PBAE-based CANs by aza-Michael addition. (c) ATR-FTIR spectra of PBAE-based CANs.

groups in the α -position of the carbonyl group,^{30,31} or (4) using internal tertiary amines.^{32,33}

Poly(β -amino esters) (PBAEs) are a unique class of polyesters that have been extensively investigated for biomedical applications, because their coexisting ester and tertiary amine groups can provide hydrolytic degradation and charge reversibility, respectively.^{34,35} More recently, PBAEs were considered for developing main-chain liquid crystal elastomers.^{36–40} PBAEs can be easily synthesized by aza-Michael addition involving the conjugated addition of a nucleophile (e.g., amine) to an electron-deficient alkene (e.g., acrylate) (Figure 2a). This reaction shares some important features of click chemistry, such as mild reaction conditions and high conversion.⁴¹ During aza-Michael reactions, multiple tertiary amines are generated *in situ* in PBAEs, which is attractive for creating catalyst-free CANs. Recently, Du Prez and coworkers reported catalyst-free PBAE-based CANs, highlighting the coexistence of both associative and dissociative bond exchanges.⁴² More specifically, the β -amino ester group in the PBAE could not only undergo a transesterification with an alcohol via an associative exchange reaction but also rearrange via a dissociation linked to the retro-aza-Michael reaction at elevated temperatures.⁴³ More recently, the Caillol research group showed that incorporating a β -hydroxyl group in PBAE-based CANs leads to a lower reprocessing temperature compared to the non-hydroxylated analogues.⁴⁴

To further develop knowledge about this interesting but rarely explored class of CANs, we herein synthesized a series of PBAE-based CANs containing various contents of β -hydroxyl groups and systematically investigated their thermal, mechanical, and dynamic properties. Increasing the content of β -hydroxyl groups leads to a higher glass transition temperature (T_g) and stronger mechanical properties owing to additional hydrogen bonding in the network. All the PBAE-based CANs could undergo catalyst-free stress relaxation because the numerous tertiary amines enhance electrophilicity of the ester group. Meanwhile, a larger number of β -hydroxyl groups in these CANs further accelerate network exchanges due to the synergistic effect of associative and dissociative reactions (transesterification at lower temperature and dynamic aza-Michael reaction at higher temperature, respectively). In terms of characteristic relaxation at 160 °C, the PBAE-based CANs with β -hydroxyl groups relaxed approximately 16–50 times faster than the non-hydroxylated CANs. Considering these dynamic properties, we further demonstrated melt reprocessing, healing, shape memory, and shape reconfiguration of PBAE-based CANs.

EXPERIMENTAL SECTION

Materials. Bisphenol A ethoxylate diacrylate (EO/phenol 1.5) (BE) and bisphenol A glycerolate (1 glycerol/phenol) diacrylate (BG) were purchased from Sigma-Aldrich. Tris(2-aminoethyl)amine (TA, >97%) was purchased from Alfa Aesar. *N,N*-Dimethylformamide (DMF) was purchased from Daejung Chemicals and Metals. All the materials were used as received.

Synthesis of PBAE-Based CANs. Four different PBAE-based CANs were synthesized by a one-pot aza-Michael reaction between diacrylate monomers (BE and/or BG) and triamine (TA) while preserving the equivalent functionality between acrylate and amine for all samples. In a representative reaction, BE (0.5 g, 1.07 mmol), BG (1.03 g, 2.13 mmol), and TA (0.15 g, 1.07 mmol) were added to a 20 mL vial. Subsequently, 10 mL of DMF was introduced into the vial, and the reagents were dissolved and vigorously mixed using a vortex mixer. The obtained solution was cast on a Teflon sheet and placed

on a hot plate (100 °C) for 24 h to allow both the aza-Michael reaction and solvent evaporation. The product film was post-cured at 140 °C for 1 h under 15 MPa to obtain a homogeneous film with uniform thickness (400 μ m, controlled using an aluminum spacer). The other PBAE-based CANs were prepared using the same protocol, except that the feed ratio of BE to BG was adjusted to control the number of hydroxyl groups in the final product. Details of the amounts of BE, BG, and TA used in the experiments are specified in Table S1.

Characterization. Attenuated total reflectance Fourier transform infrared (ATR-FTIR) spectra were recorded on a Jasco FTIR-4600 spectrometer from 650 to 4000 cm^{-1} with a resolution of 4 cm^{-1} . The background spectrum (64 scans at 4 cm^{-1} resolution) of a clean ATR crystal was used as a reference. Differential scanning calorimetry (DSC) measurements were performed using a Discovery DSC 25 (TA Instruments) under nitrogen atmosphere. The sample (~5 mg) was heated to 150 °C, cooled to –50 °C, and then reheated to 150 °C at a ramp rate of 10 °C/min. Thermogravimetric analysis (TGA) was conducted using Q50 (TA Instruments) with a platinum pan under nitrogen atmosphere. The sample (~7 mg) was heated to 800 °C at a rate of 10 °C/min. Stress–strain measurements were performed on a universal testing machine (Dr TECH, DR-100) using rectangular films (15 mm (L) \times 5 mm (W) \times 0.4 mm (T)) at an elongation rate of 50 mm/min and room temperature.

Viscoelastic measurements were performed on a dynamic mechanical analyzer (TA Instruments, DMA Q850) using a tensile clamp. Rectangular specimens with dimensions of 7 mm (L) \times 5 mm (W) \times 0.4 mm (T) were used for all experiments. These specimens were heated from –25 to 200 °C at a heating rate of 3 °C/min under an amplitude of 8 μ m at a constant frequency of 1 Hz. T_g was determined from the maximum peak in the $\tan \delta$ curve. The crosslink density (ν_e) of each sample was calculated from the rubbery modulus (E') at 120 °C using eq 1:

$$\nu_e = \frac{E'}{3RT} \quad (1)$$

Small-amplitude oscillatory shear (SAOS) and stress-relaxation measurements were performed on a strain-controlled rheometer (TA Instruments, ARES-G2) equipped with a 13 mm parallel-plate geometry under a nitrogen environment. The measurements were conducted at a strain amplitude of 0.02 and temperatures between 30 and 170 °C in 10 °C intervals. Pseudo-master curves of the SAOS and stress-relaxation data were obtained using time–temperature superposition (TTS) at a reference temperature (T_{ref}) of 110 °C.

Gel Fraction. The gel fraction was determined by Soxhlet extraction. The samples (~100 mg) were placed inside the thimble of a Soxhlet extractor and extracted with tetrahydrofuran (THF) for 24 h. Samples after extraction were dried in a vacuum oven overnight at 40 °C. The gel fraction (G_f) was calculated using eq 2:

$$G_f(\%) = \frac{W_i}{W_d} \times 100(\%) \quad (2)$$

where W_i is the initial mass of the sample and W_d is the dried mass after extraction.

Swelling Ratio. A rectangular-shaped film (~100 mg) placed inside a 20 mL vial was immersed in various solvents (ethyl acetate, dimethylformaldehyde, and chloroform) for 3 days at room temperature to reach the swelling equilibrium. The mass of the swollen films was measured after wiping the residual solvent from the surface of the films. The swelling ratio (S_r) was calculated using eq 3:

$$S_r(\%) = \frac{W_s - W_i}{W_i} \times 100(\%) \quad (3)$$

where W_i and W_s are the weights of the swollen film and the initial dried film, respectively.

Healing Experiment. For the healing experiment, a film sample (400 μ m in thick) was scratched using a razor blade and then placed inside a preheated convection oven (120 °C) for 5 min while being pressed under a glass slide (4.7 g). A laser scanning confocal

Table 1. Characterization of PBAE-Based CANs

sample	$G_r(\%)^a$	$T_d(^{\circ}\text{C})^b$	$T_g^{\text{DSC}}(^{\circ}\text{C})^c$	$T_g^{\text{DMA}}(^{\circ}\text{C})^d$	$\nu_e(\text{mol}/\text{m}^3)^e$	tensile strength (MPa) f	strain at break (%) f	Young's modulus (MPa) f
(i) BE ₀ /BG ₃	93 ± 3.7	232	53	57	0.69	29	10	617
(ii) BE ₁ /BG ₂	94 ± 2.3	238	44	50	1.05	13	41	367
(iii) BE ₂ /BG ₁	90 ± 2.3	258	37	46	0.99	8	95	150
(iv) BE ₃ /BG ₀	93 ± 1.1	270	18	36	0.73	5	178	87

^aDetermined by comparing the mass before and after extraction in THF. ^bTemperature at which 5% weight loss occurred. ^cDetermined in the second heating during DSC at a rate of 10 °C/min. ^dDetermined from the maximum of the tan δ curve. ^eCalculated from the storage modulus at 120 °C. ^fDetermined from the stress–strain curves.

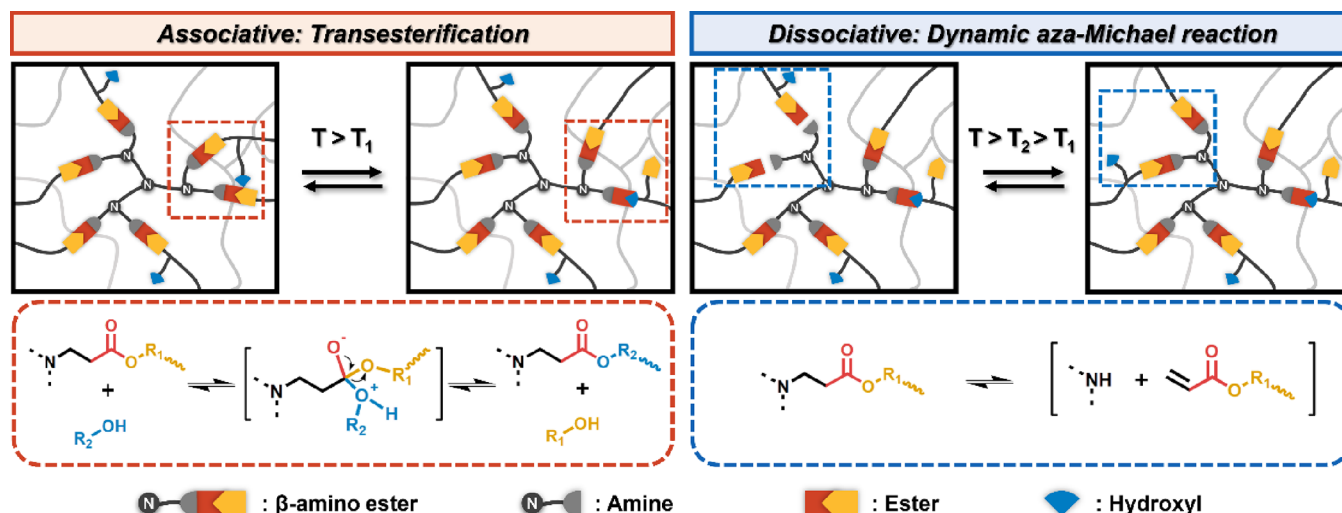


Figure 3. Schematics of dual network exchanges via transesterification (associative type) at lower temperature and dynamic aza-Michael reaction (dissociative type) at higher temperature. T_1 and T_2 represent the temperatures above which transesterification and dynamic aza-Michael reaction take place, respectively.

microscope (Olympus OLS5000) was used to measure the scratch depth before and after healing.

Quantitative Tests of Shape Memory and Shape Reconfiguration. Cyclic analyses of thermomechanical shape memory and shape reconfiguration were performed using DMA Q850 (TA Instruments) with a controlled force mode and a tension film clamp. The film specimen with a dimension of 7 mm (L) × 5 mm (W) × 0.4 mm (T) was prepared for the measurement. At first, a shape memory cycle was created using the following method. The sample was first equilibrated at 80 °C ($T > T_g$) for 3 min and then stretched at 80 °C by ramping the stress from the preload to 0.3 MPa at a rate of 0.06 MPa/min. The stretched sample was cooled to 0 °C ($T < T_g$) at a rate of 5 °C/min under a constant stress of 0.3 MPa. Subsequently, the applied stress was removed at a rate of 0.06 MPa/min to fix the temporary shape. Finally, the sample was reheated to 80 °C at a rate of 5 °C/min to trigger the shape recovery. Next, to create a shape reconfiguration cycle, the sample was further heated to 140 °C, and its permanent shape was reconfigured by stretching at a stress ramp of 0.01 MPa/min to reach 0.1 MPa and equilibrating for 20 min. The applied stress was removed, and the sample was cooled to 80 °C to form a new permanent shape. The shape memory and shape reconfiguration cycles were repeated at least twice each. Parameters for shape memory behavior (shape fixity ratio (R_f) and shape recovery ratio (R_r)) and shape reconfiguration behavior (shape retention ratio (R_{ret})) were determined using eqs 4–6:^{45,46}

$$R_f = \frac{\epsilon_u}{\epsilon_1} \times 100 (\%) \quad (4)$$

$$R_r = \frac{\epsilon_u - \epsilon_r}{\epsilon_1} \times 100 (\%) \quad (5)$$

$$R_{\text{ret}} = \frac{\epsilon_{\text{unload}}}{\epsilon_{\text{load}}} \times 100 (\%) \quad (6)$$

where ϵ_1 is the maximum strain under load before unloading, ϵ_u is the strain after cooling and unloading, and ϵ_r is the strain after recovery measured during the shape memory cycle. ϵ_{load} and ϵ_{unload} are the strains before and after load removal, respectively, measured during the shape reconfiguration cycle.

RESULTS AND DISCUSSION

Synthesis and Characterization of PBAE-Based CANs.

A series of PBAE-based CANs were synthesized by solution casting mixtures containing diacrylate monomers (BE and BG), a triamine crosslinker (TA), and DMF onto a Teflon sheet, followed by heating at 100 °C for 24 h to allow crosslinking by aza-Michael reaction. The prepared film was further cured at 140 °C for 1 h using a heat press to ensure complete crosslinking, resulting in a homogeneous film with uniform thickness (Figure 2b). According to our molecular design, the two diacrylate-functionalized monomers consist of the same bisphenol A in the central part but different types of linkers between bisphenol A and diacrylate end groups (i.e., ethoxylate for BE and glycerolate for BG). In particular, the CANs were prepared with different ratios between the BE and BG monomers, while the stoichiometric amounts of acrylates and amines were preserved. Thus, the impact of β -hydroxyl group concentration on the material properties could be investigated. Four different PBAE-based CANs were prepared and referred to as BE_x/BG_y, where x and y represent the molar ratios of BE and BG monomers, respectively.

The prepared PBAE-based CANs and starting materials were first characterized by ATR-FTIR spectroscopy, as shown in Figure 2c and Figure S1. After curing, the spectral peaks at 810 cm^{-1} (associated with the acrylate peaks in BE and BG) and 3355 cm^{-1} (due to primary amines in TA) completely disappeared. In addition, the broad peak at 3350 cm^{-1} attributed to hydroxyl groups became more pronounced with increasing BG content in the CANs. The gel fraction was greater than 93% in the PBAE-based CANs after Soxhlet extraction, indicating sufficient crosslinking (Table 1). In addition, the PBAE-based CAN exhibited excellent solvent resistance, thanks to the crosslinked structure, as suggested by the results of the swelling test in chloroform, dimethylformamide, and ethyl acetate (Figure S2). These results suggest the successful synthesis of PBAE-based CANs containing different amounts of hydroxyl groups.

What is intriguing is that these CANs (especially those bearing hydroxyl groups) are expected to undergo network exchange via both transesterification (associative type) and dynamic aza-Michael reaction (dissociative type) at elevated temperatures even without using an external catalyst, as illustrated in Figure 3. The coexistence of both mechanisms in PBAE-based CANs was first reported by Du Prez and coworkers,⁴² where transesterification and dynamic aza-Michael reactions occurred at lower temperatures (above T_1) and higher temperatures (above T_2), respectively. Later, we will discuss details of such network exchange behavior, while the primary focus here is systematically investigating the impact of β -hydroxyl group concentration on the thermal, mechanical, and dynamic properties of PBAE-based CANs.

Thermal, Mechanical, and Viscoelastic Properties.

Stress–strain curves were measured at room temperature, and the results are shown in Figure 4a and Table 1. Apparently, a higher BG content in the PBAE-based CANs led to a higher Young's modulus and tensile strength while reducing the elongation. These results originate from the different molecular

structures between the BE and BG monomers. Specifically, BE consists of flexible ethylene glycol linkers, whereas the 2-hydroxypropoxy (or glycerolate) linker in BG is less flexible but allows hydrogen bonding.^{47,48} Accordingly, a higher BG content results in a stronger network. T_g values of the PBAE-based CANs determined by DSC and DMA further support the measured mechanical properties. As shown in Figure 4b,c, increasing the BG content in the PBAE-based CANs gradually increased the T_g . Again, the higher T_g at a higher BG content was associated with a reduced flexibility and greater ability for hydrogen bonding in the resulting PBAE-based CANs. Meanwhile, the crosslinking densities calculated at the rubbery plateau temperature were fairly comparable to each other regardless of the monomer composition (Figure 4c and Table 1). Interestingly, all networks showed an approximately 10-fold decline in the storage modulus at above $150\text{ }^\circ\text{C}$, indicating a reduction in the crosslinking density. The decrease in storage modulus (or crosslinking density) originates from the dissociative dynamic aza-Michael reaction.⁴² From the TGA data, the onset degradation temperatures (T_d) of PBAE-based CANs were in the range of $230\text{--}270\text{ }^\circ\text{C}$, suggesting reasonably high thermal stability (Figure S3 and Table 1). The above results clearly suggest that the thermal, mechanical, and viscoelastic properties of PBAE-based CANs can be effectively tailored by simply adjusting the relative composition of BE and BG monomers within the network.

Rheological and Dynamic Properties. To investigate the dynamic behavior of PBAE-based CANs over a wide timescale range, pseudo-master curves of SAOS and stress-relaxation data were obtained using the TTS principle with $T_{\text{ref}} = 110\text{ }^\circ\text{C}$ (Figure 5). The two master curves were constructed using the same horizontal shift factor (a_T), and Figures S4 and S5 display the data at each measurement temperature. Figure 5a shows the linear viscoelastic properties of the elastic and viscous moduli (G' and G'' , respectively) as functions of the reduced angular frequency ($a_T\omega$). At $a_T\omega > \omega_g$, the glassy regimes are identified as $G' > G''$, where both the network exchange and chain motion are frozen. The frequency range between ω_g and ω_p is assigned to the transition regime, because segmental relaxation caused by T_g starts to occur there. This transition regime is shifted toward lower frequencies with increasing BG content due to a higher T_g (according to the DSC and DMA results in Figure 4). As $a_T\omega$ decreases below ω_p , broad plateaus develop in G' . In the early stage of this plateau regime, network integrity is maintained due to insufficient chain mobility. However, with a further decrease in frequency, the network topology is affected by more extensive dynamic rearrangement caused by transesterification and/or the aza-Michael reaction. Finally, the flow (or terminal) regime occurs at $a_T\omega < 10^{-4}\text{ rad/s}$ because the relaxation modulus (G) in Figure 5b exhibits complete stress relaxation at $t/a_T > 10^4\text{ s}$. The identification of the flow regime clearly suggests that the PBAE-based CANs can undergo efficient stress relaxation without the aid of an external catalyst, thanks to the NGP effect (i.e., ester bonds activated by the neighboring β -amino and β -hydroxyl moieties).^{42,44} Interestingly, BE₃/BG₀, which lacks hydroxyl moieties, exhibited the slowest relaxation despite the lowest T_g . This is probably because its relaxation is only driven by the aza-Michael reaction, while the other CANs also undergo relaxation through transesterification. Note that network exchange due to the aza-Michael reaction is slower than that due to transesterification.⁴²

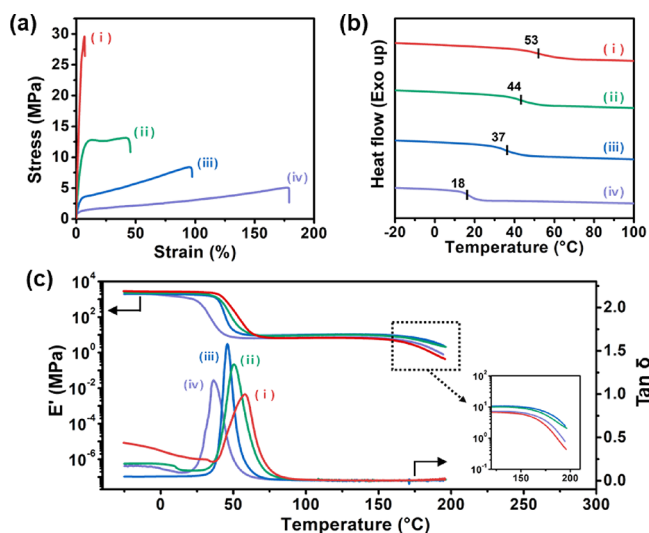


Figure 4. (a) Stress–strain curves, (b) DSC curves in the second heating, and (c) viscoelastic properties of PBAE-based CANs: (i) BE₀/BG₃, (ii) BE₁/BG₂, (iii) BE₂/BG₁, and (iv) BE₃/BG₀. Refer to the sample name in Table 1 where BE and BG represent bisphenol A ethoxylate diacrylate and bisphenol A glycerolate diacrylate, respectively, while the numbers are the molar ratios of BE and BG monomers.

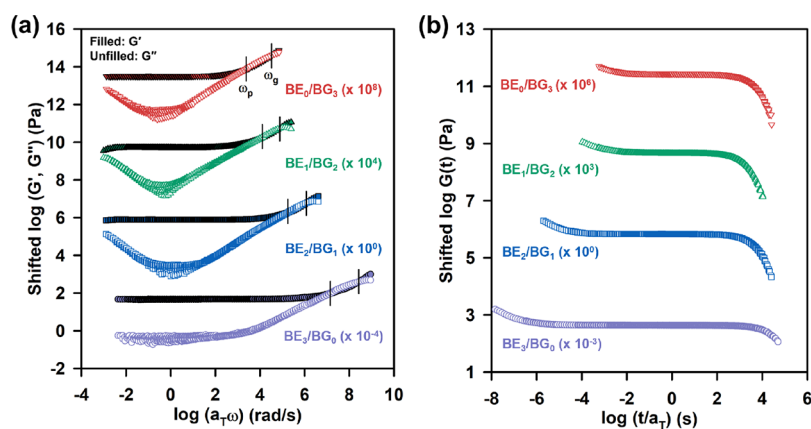


Figure 5. Pseudo-master curves of (a) elastic and viscous moduli (G' and G'' vs $a_T \omega$, respectively) and (b) stress-relaxation modulus (G vs t/a_T) at $T_{\text{ref}} = 110$ °C for PBAE-based CANs. The moduli are artificially shifted vertically to allow easy comparison.

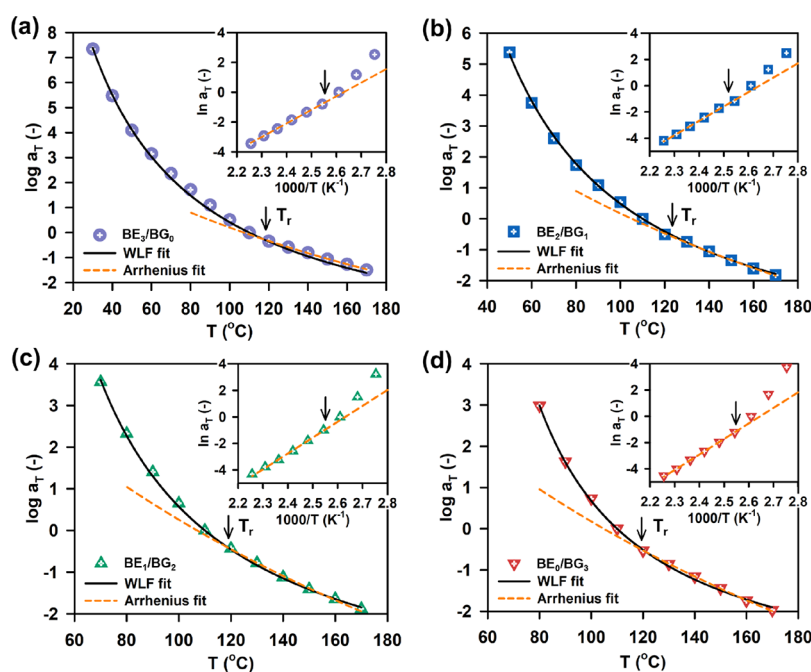


Figure 6. (a–d) Horizontal shift factors (a_T) as a function of temperature with $T_{\text{ref}} = 110$ °C for PBAE-based CANs. Black solid lines, the WLF fit; orange dashed lines, the Arrhenius fit; arrows, reprocessing temperature (T_r) determined from the crossover between the WLF and Arrhenius fits. Above T_r , the network rearrangement rate is mainly dominated by the exchange reactions. The insets are plots of $\ln a_T$ vs $1000/T$ to highlight that a_T follows Arrhenius-type behavior at $T > T_r$.

Figure 6 shows the temperature dependence of the horizontal shift factor (a_T) for the PBAE-based CANs. To describe the temperature dependence of a_T , we fitted the data with the Williams–Landel–Ferry (WLF) equation for the entire temperature range and the Arrhenius equation for temperatures between 120 and 170 °C. The corresponding equations and fitting parameters are listed in Table S2. The a_T values are described well by the WLF equation over the entire temperature range. However, a careful examination of the high-temperature regime (>120 °C) suggests that a_T follows an Arrhenius relationship there. Thus, the temperature dependence of a_T shows a transition from the WLF-type to Arrhenius-type at ~ 120 °C. Previous experiments and computer simulation also indicated such a transition of the temperature dependence.^{24,49–54} The transition to the Arrhenius behavior at ~ 120 °C is distinguished from a well-known Arrhenius approximation of the WLF at temperatures above $T_g + 100$ °C.

While $T_{g\text{-DSC}} + 100$ °C values of four PBAE-based CANs are ≥ 120 °C and increase with the amount of the BG monomers, the onset of the Arrhenius-type behavior is observed consistently at ~ 120 °C. Thus, bond exchange mechanisms influence the Arrhenius-type behavior of the current CANs.

The WLF-type behavior at temperatures below 120 °C was mainly due to the low mobility of network strands and segments, suggesting a diffusion-limited regime.^{49,51} Above 120 °C, the dominance of network rearrangement shifts the system from a diffusion-limited regime to a reaction-limited one, as revealed by the Arrhenius-type behavior. Thus, rheological measurements indicate that the temperature dependence of macroscopic characteristics of CANs changes from a diffusion-limited regime to a reaction-limited regime. Motivated by this, we calculated the crossover temperature between the two regimes and defined it as the reprocessing temperature (T_r) (Figure 6). Thus, the T_r is an empirical temperature where

control of the overall bond exchange rate shifts from diffusion-limited to reaction-limited. The T_r is conceptually similar to the topology freezing temperature in the vitrimers. However, while the topology freezing temperature is not theoretically robust and is somewhat hypothetical,⁵⁵ we consider the T_r as a processing-friendly parameter than an absolute threshold. The calculated T_r is ~ 120 °C for all the PBAE-based CANs.

Next, characteristic relaxation times (τ) of the PBAE-based CANs were obtained by fitting the normalized stress-relaxation data (G/G_0 vs t) with stretched exponential equations in the temperature range of 120–160 °C (Figure S6). The corresponding fitting parameters are listed in Table S2. Figure 7a shows an Arrhenius plot of τ . Because the τ values follow an

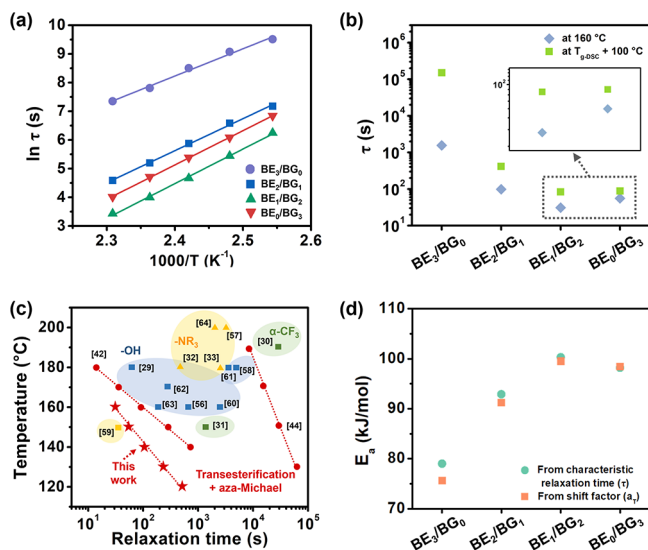


Figure 7. (a) Arrhenius plot obtained from characteristic relaxation times (τ) at different temperatures. Rheological activation energies (E_a) are extracted from the slopes of the solid fitting lines. (b) τ values at $T = 160$ °C or $T_{g-DSC} + 100$ °C. (c) Comparison of relaxation times between BE_1/BG_2 and reported catalyst-free transesterification-based CANs. (d) E_a values obtained from τ and a_T at different BG molar ratios.

Arrhenius relation with a_T , the rheological activation energy (E_a) could be extracted from the slope of the Arrhenius plot.

The relaxation time is significantly affected by the concentration of hydroxyl groups in the PBAE-based CANs (Figure 7b and Table 2). Specifically, more hydroxyl groups

Table 2. Characteristic Relaxation Time and Rheological Activation Energy According to Data in Figure 5

sample	τ (s)		E_a (kJ/mol)	
	at 160 °C	at $T_{g-DSC} + 100$ °C	from τ	from a_T
BE_3/BG_0	1.56×10^3	1.50×10^4	79.0	75.6
BE_2/BG_1	9.84×10^1	4.16×10^2	92.9	91.2
BE_1/BG_2	3.10×10^1	8.37×10^1	100.3	99.5
BE_0/BG_3	5.54×10^1	8.87×10^1	98.2	98.4

likely lead to faster stress relaxation (i.e., faster network exchange) perhaps due to accelerated transesterification. Compared to catalyst-free transesterification-based CANs reported so far, the PBAE-based CANs containing sufficiently large amounts of hydroxyl groups (e.g., BE_1/BG_2) display one of the fastest stress-relaxation times because of the synergistic

effects of transesterification and dynamic aza-Michael reaction (Figure 7c and Table S4).^{29–33,42,44,56–64} Note that the concentration of tertiary amines in our PBAE-based CANs is also relatively higher compared to other similarly designed CANs,^{42,44} and this may also contribute to faster relaxation. Interestingly, the relaxation of BE_0/BG_3 was slightly slower than that of BE_1/BG_2 despite a larger number of hydroxyl groups, when their τ values were compared at 160 °C (Figure 7b). The same trend was observed at other temperatures (Figure 7a). This behavior is attributed to different amounts of free volume in each network, as implied by their different T_g values in the DSC results. While the relaxation of PBAE-based CANs is mainly triggered by transesterification and dynamic aza-Michael reaction, segmental motion of the networks is equally important in the overall relaxation behavior and should be considered as well. Therefore, the relaxation times at $T_{g-DSC} + 100$ °C, corresponding to the iso-free-volume state of the PBAE-based CANs, were also compared (Figure 7b). After correcting for the free volume, BE_1/BG_2 and BE_0/BG_3 displayed comparable τ values, suggesting that their difference in τ at 160 °C was not due to different bond exchange rates but rather different T_g values. This highlights the need to correct the free volume effect before evaluating the exchange reaction rates from the rheological parameters. We speculate that the comparable relaxation rates between BE_1/BG_2 and BE_0/BG_3 in the iso-free-volume state are related to the local molecular environment for transesterification, namely, the similar probability of hydroxyl groups to react with surrounding esters in these two CANs.

The activation energy (E_a), which describes the sensitivity of stress relaxation to temperature changes, can be extracted from the slopes of temperature vs relaxation time, as well as the slopes of temperature vs shift factor. The E_a values obtained from two methods are in excellent agreement with each other (Figure 7d and Table 2). Interestingly, E_a as a function of BG composition displays the opposite trend to that of τ (i.e., a higher BG composition leads to a higher E_a and lower τ , except for BE_0/BG_3) while both displaying a strong dependence on the concentration of β -hydroxyl groups in the PBAE-based CANs. This result again supports the synergistic effects of transesterification and dynamic aza-Michael reaction.

Reprocessing, Healing, Shape Memory, and Shape Reconfiguration. After exploring the thermal, mechanical, and dynamic properties of PBAE-based CANs, we focus on BE_0/BG_3 , which exhibits fast relaxation with the highest mechanical properties, as a representative to demonstrate the capabilities of melt reprocessing, healing, shape memory, and shape reconfiguration. First, Figure 8a displays photographs captured during melt reprocessing: a pristine sample was cut into multiple segments and then hot-pressed at 140 °C under 15 MPa for 30 min. Note that BE_0/BG_3 could be reprocessed at a temperature approximately 20 °C lower than that of BE_3/BG_0 (160 °C) owing to its faster stress relaxation (Figure S7). Although no discernible change in the chemical structure was detected in the ATR-FTIR spectra after reprocessing, repeated reprocessing gradually degraded the mechanical properties likely due to thermo-oxidative degradation (Figures S8 and S9).^{65,66} Indeed, adding 2 wt % butylated hydroxytoluene (BHT) as an antioxidant not only improved the mechanical properties of a pristine sample but also slowed down the degradation of mechanical properties (Figure S9 and Table S5). Second, thermally induced healing of BE_0/BG_3 was demonstrated by scratching the sample using a razor blade (78

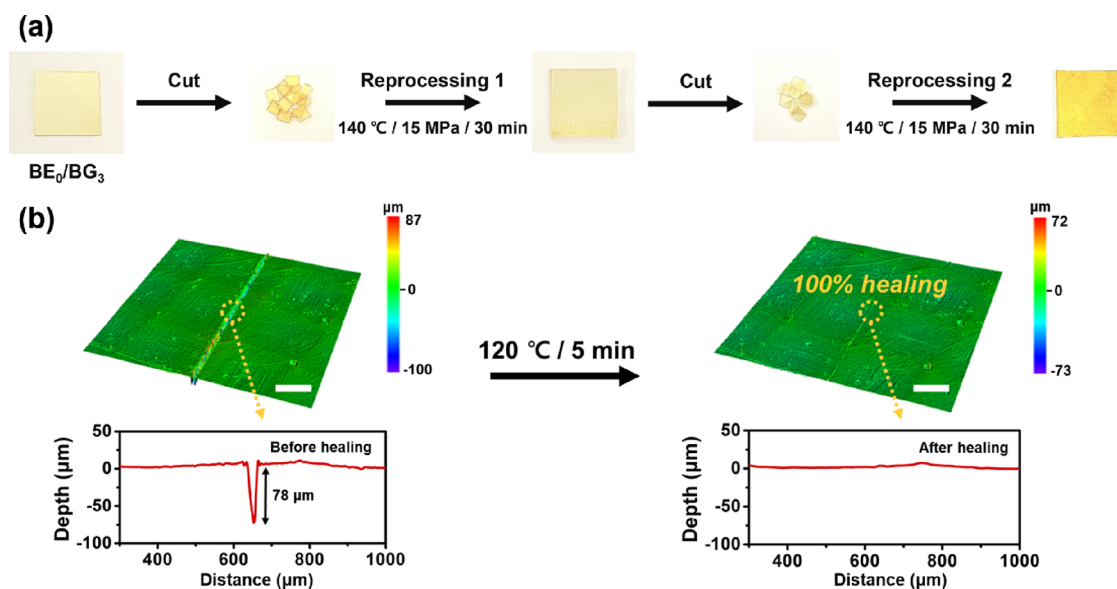


Figure 8. Reprocessing and healing properties of BE₀/BG₃ as a representative sample. (a) Photographs captured during two consecutive melt-reprocessing. (b) 3D laser confocal micrographs and the corresponding depth profiles before and after healing (scale bar = 50 μm).

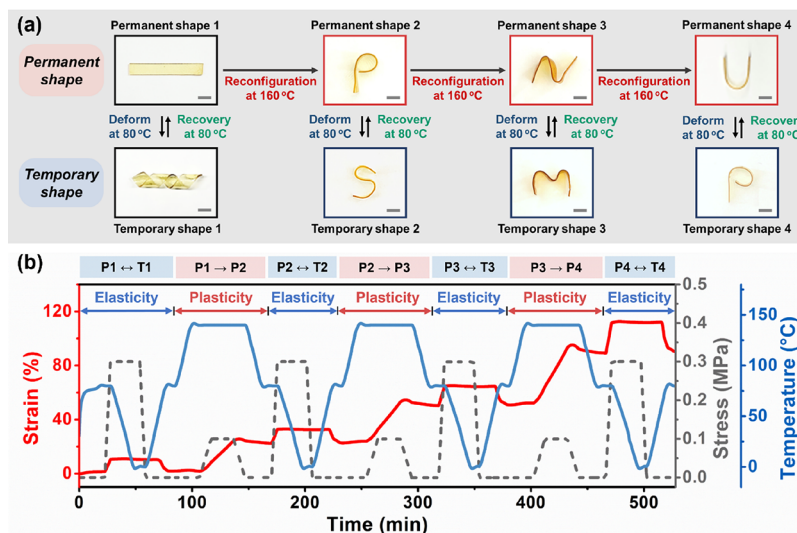


Figure 9. (a) Qualitative demonstration of shape memory and shape reconfiguration (scale bar = 5 mm). (b) Consecutive cycles of elasticity-based shape memory and plasticity-based shape reconfiguration. In this panel, P and T indicate permanent shape and temporary shape, respectively.

μm depth) and subsequently placing it in a convention oven (120 °C) for 5 min (Figure 8b) under gentle pressure from a glass slide (4.7 g). After heating, observation using a laser confocal microscope revealed that the scratch fully disappeared and the initial flat surface was recovered. The abilities of melt reprocessing and healing both originate from the efficient network rearrangement within BE₀/BG₃.

Although conventional thermoset shape memory polymers (SMPs) show excellent shape recovery capability driven by entropy elasticity, they can only retain a single permanent shape, i.e., a thermodynamically equilibrated shape determined during the crosslinking process. However, if the macromolecular network of SMPs can be rearranged under external stimuli, the permanent shape can be redefined through the plasticity of polymers.^{67,68} The inherent network elasticity as well as the plasticity (activated above T_i) in the PBAE-based CANs allows for both shape memory and shape reconfiguration, as demonstrated in Figure 9a and Video S1. For instance,

a rectangular film (permanent shape 1) was heated at 80 °C ($T > T_g$), reshaped into a twisted form (temporary shape 1), and subsequently cooled to 10 °C ($T < T_g$) to fix this temporary shape. When the sample was reheated to 80 °C, permanent shape 1 was successfully recovered through elasticity, suggesting an effective one-way shape memory effect. For shape reconfiguration, the same rectangular film (permanent shape 1) was mechanically deformed into the shape of letter "P" at 160 °C ($T > T_i$). By holding this shape for 10 min at this temperature, the "P" shape became the new equilibrated shape (permanent shape 2) induced by network rearrangement, and this shape was preserved when cooled to room temperature. A letter "N" shape (permanent shape 3) and a "U" shape (permanent shape 4) were also obtained using the same protocol. All reconfigured permanent shapes exhibited excellent one-way shape memory behavior using T_g as the switching temperature (i.e., the shape recovers from the temporarily fixed ones ("S", "M", and "P", bottom row of

Figure 9a) to the corresponding permanent ones (“P”, “N”, and “U”, top row)). Both the elasticity-based shape memory and plasticity-based shape reconfiguration were analyzed using DMA, by monitoring the strain response while programming the stress and temperature (Figure 9b). Quantitative analyses of consecutive cycles of shape memory and shape reconfiguration revealed excellent shape fixing (>95%), shape recovery (>94%), and shape retention ratio (>92%) (Table S6). The ability to redefine the permanent shape of a single polymer network through exchangeable bonds offers unique freedom for shape manipulation and controllable shape-changing behavior.

CONCLUSIONS

In summary, a series of PBAE-based CANs were synthesized by one-pot aza-Michael addition using bisphenol A ethoxylate diacrylate (BE), bisphenol A glycerolate diacrylate (BG), and a triamine crosslinker. Upon increasing the BG ratio used in synthesis, both the glass transition temperature and mechanical properties of the resulting PBAE-based CANs increased due to enhanced hydrogen bonding. The presence of multiple tertiary amines in the PBAE-based CANs allowed stress relaxation through a dynamic aza-Michael reaction in the absence of an external catalyst. At the same time, transesterification also occurred when the system contained β -hydroxyl groups. Interestingly, the overall stress-relaxation rate could be accelerated by increasing the amount of β -hydroxyl groups due to synergistic effects from both transesterification (associative pathway) and dynamic aza-Michael reaction (dissociative pathway), as revealed by a thorough rheological investigation with careful consideration of segmental motion of the networks. The characteristic relaxation time of PBAE-based CANs containing a sufficient amount of β -hydroxyl groups was one of the fastest among catalyst-free transesterification-based CANs developed so far. Based on the dynamic features, we successfully demonstrated melt reprocessing and healing at elevated temperatures under mild pressure, as well as shape memory and shape reconfiguration. Considering the facile synthesis of PBAE-based CANs and their tunable thermal, mechanical, and dynamic properties according to the β -hydroxyl group concentration within the network, these CANs can provide useful guidelines for designing materials that are mechanically robust, sustainable, and capable of fast reprocessing.

ASSOCIATED CONTENT

Supporting Information

The Supporting Information is available free of charge at <https://pubs.acs.org/doi/10.1021/acs.macromol.2c01872>.

ATR-FTIR spectra of monomers, swelling ratio, TGA thermograms, SAOS and stress-relaxation data, fitting parameters of WLF and Arrhenius equations, normalized stress-relaxation modulus, fitting parameters of the stretched exponential function, photographs captured during melt reprocessing, ATR-FTIR spectra before and after reprocessing, S–S curves before and after reprocessing, quantitative evaluation of shape memory, and shape reconfiguration properties (PDF)

Movie S1: Thermally induced shape memory behavior of BE0/BG3. An original permanent shape 1 (a linear shape) and three reconfigured permanent shapes (“P” for permanent shape 2, “N” for permanent shape 3, and

“U” for permanent shape 4) were recovered from four corresponding temporary shapes (a twisted shape for temporary shape 1, “S” for temporary shape 2, “M” for temporary shape 3, and “P” for temporary shape 4) by immersing in a water bath (80 °C) (MP4)

AUTHOR INFORMATION

Corresponding Authors

Kyu Hyun — School of Chemical Engineering and Institute for Environment and Energy, Pusan National University, Busan 46241, Republic of Korea; orcid.org/0000-0001-5129-5169; Email: kyuhyun@pusan.ac.kr

Suk-kyun Ahn — School of Chemical Engineering and Department of Polymer Science and Engineering, Pusan National University, Busan 46241, Republic of Korea; orcid.org/0000-0002-6841-4213; Email: skahn@pusan.ac.kr

Authors

Gyuri Lee — School of Chemical Engineering, Pusan National University, Busan 46241, Republic of Korea

Hyeong Yong Song — Institute for Environment and Energy, Pusan National University, Busan 46241, Republic of Korea

Subi Choi — School of Chemical Engineering, Pusan National University, Busan 46241, Republic of Korea

Chae Bin Kim — School of Chemical Engineering and Department of Polymer Science and Engineering, Pusan National University, Busan 46241, Republic of Korea; orcid.org/0000-0002-7976-7612

Complete contact information is available at:

<https://pubs.acs.org/doi/10.1021/acs.macromol.2c01872>

Author Contributions

#G.L. and H.Y.S. contributed equally to this work.

Notes

The authors declare no competing financial interest.

ACKNOWLEDGMENTS

This work was supported by National Research Foundation of Korea (NRF) grants funded by the Korean Government, Ministry of Science, and ICT (MSIT) (2019R1C1C1006048 and 2021M3H4A1A03041403). G.L. and S.C. acknowledge the BK FOUR Program for their partial financial support.

REFERENCES

- (1) Garcia, J. M.; Robertson, M. L. The future of plastics recycling. *Science* **2017**, 358, 870–872.
- (2) Kloxin, C. J.; Scott, T. F.; Adzima, B. J.; Bowman, C. N. Covalent Adaptable Networks (CANs): A Unique Paradigm in Cross-Linked Polymers. *Macromolecules* **2010**, 43, 2643–2653.
- (3) Samanta, S.; Kim, S.; Saito, T.; Sokolov, A. P. Polymers with Dynamic Bonds: Adaptive Functional Materials for a Sustainable Future. *J. Phys. Chem. B* **2021**, 125, 9389–9401.
- (4) Zheng, J.; Png, Z. M.; Ng, S. H.; Tham, G. X.; Ye, E.; Goh, S. S.; Loh, X. J.; Li, Z. Vitrimers: Current research trends and their emerging applications. *Mater. Today* **2021**, 51, 586–625.
- (5) Luo, J.; Demchuk, Z.; Zhao, X.; Saito, T.; Tian, M.; Sokolov, A. P.; Cao, P.-F. Elastic vitrimers: Beyond thermoplastic and thermoset elastomers. *Matter* **2022**, 5, 1391–1422.
- (6) Scheutz, G. M.; Lessard, J. J.; Sims, M. B.; Sumerlin, B. S. Adaptable Crosslinks in Polymeric Materials: Resolving the Intersection of Thermoplastics and Thermosets. *J. Am. Chem. Soc.* **2019**, 141, 16181–16196.

- (7) Chen, X.; Dam, M. A.; Ono, K.; Mal, A.; Shen, H.; Nutt, S. R.; Sheran, K.; Wudl, F. A Thermally Re-mendable Cross-Linked Polymeric Material. *Science* **2002**, *295*, 1698–1702.
- (8) Ying, H.; Zhang, Y.; Cheng, J. Dynamic urea bond for the design of reversible and self-healing polymers. *Nat. Commun.* **2014**, *5*, 3218.
- (9) Liu, W.-X.; Zhang, C.; Zhang, H.; Zhao, N.; Yu, Z.-X.; Xu, J. Oxime-Based and Catalyst-Free Dynamic Covalent Polyurethanes. *J. Am. Chem. Soc.* **2017**, *139*, 8678–8684.
- (10) Zhang, X.; Wang, S.; Jiang, Z.; Li, Y.; Jing, X. Boronic Ester Based Vitrimers with Enhanced Stability via Internal Boron–Nitrogen Coordination. *J. Am. Chem. Soc.* **2020**, *142*, 21852–21860.
- (11) Kleine, T. S.; Nguyen, N. A.; Anderson, L. E.; Namnabat, S.; LaVilla, E. A.; Showghi, S. A.; Dirlam, P. T.; Arrington, C. B.; Manchester, M. S.; Schwiegerling, J.; et al. High Refractive Index Copolymers with Improved Thermomechanical Properties via the Inverse Vulcanization of Sulfur and 1,3,5-Triisopropenylbenzene. *ACS Macro Lett.* **2016**, *5*, 1152–1156.
- (12) Zhang, B.; Digby, Z. A.; Flum, J. A.; Chakma, P.; Saul, J. M.; Sparks, J. L.; Konkolewicz, D. Dynamic Thiol–Michael Chemistry for Thermoresponsive Rehealable and Malleable Networks. *Macromolecules* **2016**, *49*, 6871–6878.
- (13) Baruah, R.; Kumar, A.; Ujjwal, R. R.; Kedia, S.; Ranjan, A.; Ojha, U. Recyclable Thermosets Based on Dynamic Amidation and Aza-Michael Addition Chemistry. *Macromolecules* **2016**, *49*, 7814–7824.
- (14) Montarnal, D.; Capelot, M.; Tournilhac, F.; Leibler, L. Silica-Like Malleable Materials from Permanent Organic Networks. *Science* **2011**, *334*, 965–968.
- (15) Mu, S.; Zhang, Y.; Zhou, J.; Wang, B.; Wang, Z. Recyclable and Mechanically Robust Palm Oil-Derived Epoxy Resins with Reconfigurable Shape-Memory Properties. *ACS Sustainable Chem. Eng.* **2020**, *8*, 5296–5304.
- (16) Yang, X.; Guo, L.; Xu, X.; Shang, S.; Liu, H. A fully bio-based epoxy vitrimer: Self-healing, triple-shape memory and reprocessing triggered by dynamic covalent bond exchange. *Mater. Des.* **2020**, *186*, No. 108248.
- (17) Denissen, W.; Rivero, G.; Nicolaÿ, R.; Leibler, L.; Winne, J. M.; Du Prez, F. E. Vinylogous Urethane Vitrimers. *Adv. Funct. Mater.* **2015**, *25* (16), 2451–2457.
- (18) Fortman, D. J.; Brutman, J. P.; Cramer, C. J.; Hillmyer, M. A.; Dichtel, W. R. Mechanically Activated, Catalyst-Free Polyhydroxyurethane Vitrimers. *J. Am. Chem. Soc.* **2015**, *137*, 14019–14022.
- (19) Snyder, R. L.; Fortman, D. J.; De Hoe, G. X.; Hillmyer, M. A.; Dichtel, W. R. Reprocessable Acid-Degradable Polycarbonate Vitrimers. *Macromolecules* **2018**, *51*, 389–397.
- (20) Taynton, P.; Ni, H.; Zhu, C.; Yu, K.; Loob, S.; Jin, Y.; Qi, H. J.; Zhang, W. Repairable Woven Carbon Fiber Composites with Full Recyclability Enabled by Malleable Polyimine Networks. *Adv. Mater.* **2016**, *28*, 2904–2909.
- (21) Kim, S.; Rahman, M. A.; Arifuzzaman, M.; Gilmer, D. B.; Li, B.; Wilt, J. K.; Lara-Curzio, E.; Saito, T. Closed-loop additive manufacturing of upcycled commodity plastic through dynamic cross-linking. *Sci. Adv.* **2022**, *8*, No. eabn6006.
- (22) Lu, Y.-X.; Tournilhac, F.; Leibler, L.; Guan, Z. Making Insoluble Polymer Networks Malleable via Olefin Metathesis. *J. Am. Chem. Soc.* **2012**, *134*, 8424–8427.
- (23) Lu, Y.-X.; Guan, Z. Olefin Metathesis for Effective Polymer Healing via Dynamic Exchange of Strong Carbon–Carbon Double Bonds. *J. Am. Chem. Soc.* **2012**, *134*, 14226–14231.
- (24) Nishimura, Y.; Chung, J.; Muradyan, H.; Guan, Z. Silyl Ether as a Robust and Thermally Stable Dynamic Covalent Motif for Malleable Polymer Design. *J. Am. Chem. Soc.* **2017**, *139*, 14881–14884.
- (25) Alabiso, W.; Schlögl, S. The Impact of Vitrimers on the Industry of the Future: Chemistry Properties and Sustainable Forward-Looking Applications. *Polymer* **2020**, *12*, 1660.
- (26) Cuminet, F.; Caillol, S.; Dantras, É.; Leclerc, É.; Ladmiral, V. Neighboring Group Participation and Internal Catalysis Effects on Exchangeable Covalent Bonds: Application to the Thriving Field of Vitrimer Chemistry. *Macromolecules* **2021**, *54*, 3927–3961.
- (27) Van Lijsebetten, F.; Holloway, J. O.; Winne, J. M.; Du Prez, F. E. Internal catalysis for dynamic covalent chemistry applications and polymer science. *Chem. Soc. Rev.* **2020**, *49*, 8425–8438.
- (28) Capelot, M.; Montarnal, D.; Tournilhac, F.; Leibler, L. Metal-Catalyzed Transesterification for Healing and Assembling of Thermosets. *J. Am. Chem. Soc.* **2012**, *134*, 7664–7667.
- (29) Delahaye, M.; Winne, J. M.; Du Prez, F. E. Internal Catalysis in Covalent Adaptable Networks: Phthalate Monoester Transesterification As a Versatile Dynamic Cross-Linking Chemistry. *J. Am. Chem. Soc.* **2019**, *141*, 15277–15287.
- (30) Cuminet, F.; Berne, D.; Lemouzy, S.; Dantras, É.; Joly-Duhamel, C.; Caillol, S.; Leclerc, É.; Ladmiral, V. Catalyst-free transesterification vitrimers: activation via α -difluoroesters. *Polym. Chem.* **2022**, *13*, 2651–2658.
- (31) Berne, D.; Cuminet, F.; Lemouzy, S.; Joly-Duhamel, C.; Poli, R.; Caillol, S.; Leclerc, É.; Ladmiral, V. Catalyst-Free Epoxy Vitrimers Based on Transesterification Internally Activated by an α -CF₃ Group. *Macromolecules* **2022**, *55*, 1669–1679.
- (32) Altuna, F. I.; Hoppe, C. E.; Williams, R. J. J. Epoxy vitrimers with a covalently bonded tertiary amine as catalyst of the transesterification reaction. *Eur. Polym. J.* **2019**, *113*, 297–304.
- (33) Hayashi, M. Dominant Factor of Bond-Exchange Rate for Catalyst-Free Polyester Vitrimers with Internal Tertiary Amine Moieties. *ACS Appl. Polym. Mater.* **2020**, *2*, 5365–5370.
- (34) Liu, Y.; Li, Y.; Keskin, D.; Shi, L. Poly(β -Amino Esters): Synthesis, Formulations, and Their Biomedical Applications. *Adv. Healthcare Mater.* **2019**, *8*, 1801359.
- (35) Iqbal, S.; Qu, Y.; Dong, Z.; Zhao, J.; Rauf Khan, A.; Rehman, S.; Zhao, Z. Poly (β -amino esters) based potential drug delivery and targeting polymer; an overview and perspectives (review). *Eur. Polym. J.* **2020**, *141*, No. 110097.
- (36) Ware, T. H.; McConney, M. E.; Wie, J. J.; Tondiglia, V. P.; White, T. J. Actuating materials. Voxelated liquid crystal elastomers. *Science* **2015**, *347*, 982–984.
- (37) Yoon, H.-H.; Kim, D.-Y.; Jeong, K.-U.; Ahn, S. K. Surface Aligned Main-Chain Liquid Crystalline Elastomers: Tailored Properties by the Choice of Amine Chain Extenders. *Macromolecules* **2018**, *51*, 1141–1149.
- (38) Kim, K.; Guo, Y.; Bae, J.; Choi, S.; Song, H. Y.; Park, S.; Hyun, K.; Ahn, S.-K. 4D Printing of Hygroscopic Liquid Crystal Elastomer Actuators. *Small* **2021**, *17*, 2100910.
- (39) Lee, J.-H.; Bae, J.; Hwang, J. H.; Choi, M.-Y.; Kim, Y. S.; Park, S.; Na, J.-H.; Kim, D.-G.; Ahn, S.-k. Robust and Reprocessable Artificial Muscles Based on Liquid Crystal Elastomers with Dynamic Thiourea Bonds. *Adv. Funct. Mater.* **2022**, *32*, 2110360.
- (40) Chen, Q.; Li, W.; Wei, Y.; Ji, Y. Reprogrammable 3D Liquid-Crystalline Actuators with Precisely Controllable Stepwise Actuation. *Adv. Intell. Syst.* **2021**, *3*, 2000249.
- (41) Konuray, A. O.; Fernández-Francos, X.; Serra, À.; Ramis, X. Sequential curing of amine-acrylate-methacrylate mixtures based on selective aza-Michael addition followed by radical photopolymerization. *Eur. Polym. J.* **2016**, *84*, 256–267.
- (42) Taplan, C.; Guerre, M.; Du Prez, F. E. Covalent Adaptable Networks Using β -Amino Esters as Thermally Reversible Building Blocks. *J. Am. Chem. Soc.* **2021**, *143*, 9140–9150.
- (43) Holloway, J. O.; Taplan, C.; Duprez, F. E. Combining vinylogous urethane and β -amino ester chemistry for dynamic material design. *Polym. Chem.* **2022**, *13*, 2008–2018.
- (44) Berne, D.; Coste, G.; Morales-Cerrada, R.; Boursier, M.; Pinaud, J.; Ladmiral, V.; Caillol, S. Taking advantage of β -hydroxy amine enhanced reactivity and functionality for the synthesis of dual covalent adaptable networks. *Polym. Chem.* **2022**, *13*, 3806–3814.
- (45) Yang, Z.; Wang, Q.; Wang, T. Dual-Trigged and Thermally Reconfigurable Shape Memory Graphene-Vitrimer Composites. *ACS Appl. Mater. Interfaces* **2016**, *8*, 21691–21699.
- (46) Wang, L.; Wu, S.; Guo, X.; Fan, J.; Zhou, S.; Chen, Z. Multi-shape-changing interpenetrating networks with shape memory effect and adaptive plastic deformations. *Appl. Mater. Today* **2021**, *25*, No. 101246.

- (47) Lemon, M. T.; Jones, M. S.; Stansbury, J. W. Hydrogen bonding interactions in methacrylate monomers and polymers. *J. Biomed. Mater. Res. A* **2007**, *83A*, 734–746.
- (48) Barszczewska-Rybarek, I. M. A Guide through the Dental Dimethacrylate Polymer Network Structural Characterization and Interpretation of Physico-Mechanical Properties. *Materials* **2019**, *12*, 4057.
- (49) Snijkers, F.; Pasquino, R.; Maffezzoli, A. Curing and viscoelasticity of vitrimers. *Soft Matter* **2017**, *13*, 258–268.
- (50) Perego, A.; Khabaz, F. Volumetric and Rheological Properties of Vitrimers: A Hybrid Molecular Dynamics and Monte Carlo Simulation Study. *Macromolecules* **2020**, *53*, 8406–8416.
- (51) Wu, J.-B.; Li, S.-J.; Liu, H.; Qian, H.-J.; Lu, Z.-Y. Dynamics and reaction kinetics of coarse-grained bulk vitrimers: a molecular dynamics study. *Phys. Chem. Chem. Phys.* **2019**, *21*, 13258–13267.
- (52) Park, J.; Song, H. Y.; Choi, S.; Ahn, S. K.; Hyun, K.; Kim, C. B. Spatiotemporal vitrimerization of a thermosetting polymer using a photo-latent catalyst for transesterification. *J. Mater. Chem. A* **2022**, *10*, 6475–6480.
- (53) Fang, H.; Ye, W.; Ding, Y.; Winter, H. H. Rheology of the Critical Transition State of an Epoxy Vitrimer. *Macromolecules* **2020**, *53*, 4855–4862.
- (54) Zych, A.; Tellers, J.; Bertolacci, L.; Ceseracciu, L.; Marini, L.; Mancini, G.; Athanassiou, A. Biobased, Biodegradable, Self-Healing Boronic Ester Vitrimers from Epoxidized Soybean Oil Acrylate. *ACS Appl. Polym. Mater.* **2021**, *3*, 1135–1144.
- (55) Guerre, M.; Taplan, C.; Winne, J. M.; Du Prez, F. E. Vitrimers: directing chemical reactivity to control material properties. *Chem. Sci.* **2020**, *11*, 4855–4870.
- (56) Debnath, S.; Kaushal, S.; Ojha, U. Catalyst-Free Partially Bio-Based Polyester Vitrimers. *ACS Appl. Polym. Mater.* **2020**, *2*, 1006–1013.
- (57) Li, Y.; Liu, T.; Zhang, S.; Shao, L.; Fei, M.; Yu, H.; Zhang, J. Catalyst-free vitrimer elastomers based on a dimeric acid: robust mechanical performance, adaptability and hydrothermal recyclability. *Green Chem.* **2020**, *22*, 870–881.
- (58) Han, J.; Liu, T.; Hao, C.; Zhang, S.; Guo, B.; Zhang, J. A Catalyst-Free Epoxy Vitrimer System Based on Multifunctional Hyperbranched Polymer. *Macromolecules* **2018**, *51*, 6789–6799.
- (59) Adjaoud, A.; Trejo-Machin, A.; Puchot, L.; Verge, P. Polybenzoxazines: a sustainable platform for the design of fast responsive and catalyst-free vitrimers based on trans-esterification exchanges. *Polym. Chem.* **2021**, *12*, 3276–3289.
- (60) Xu, Y. Z.; Fu, P.; Dai, S. L.; Zhang, H. B.; Bi, L. W.; Jiang, J. X.; Chen, Y. X. Catalyst-free self-healing fully bio-based vitrimers derived from tung oil: Strong mechanical properties, shape memory, and recyclability. *Ind. Crops Prod.* **2021**, *171*, No. 113978.
- (61) Liu, T.; Zhang, S.; Hao, C.; Verdi, C.; Liu, W.; Liu, H.; Zhang, J. Glycerol Induced Catalyst-Free Curing of Epoxy and Vitrimer Preparation. *Macromol. Rapid Commun.* **2019**, *40*, 1800889.
- (62) Liu, Y.; Yu, Z.; Xu, X.; Wang, B.; Feng, H.; Li, P.; Zhu, J.; Ma, S. Crystallizable Aliphatic Chains Enhanced Covalent Adaptable Networks: Fast Reprocessing and Improved Performance. *Macromol. Rapid Commun.* **2022**, *43*, 2200379.
- (63) Zhang, J.; Gong, Z.; Wu, C.; Li, T.; Tang, Y.; Wu, J.; Jiang, C.; Miao, M.; Zhang, D. Itaconic acid-based hyperbranched polymer toughened epoxy resins with rapid stress relaxation, superb solvent resistance and closed-loop recyclability. *Green Chem.* **2022**, *24*, 6900–6911.
- (64) Hao, C.; Liu, T.; Zhang, S.; Liu, W.; Shan, Y.; Zhang, J. Triethanolamine-Mediated Covalent Adaptable Epoxy Network: Excellent Mechanical Properties, Fast Repairing, and Easy Recycling. *Macromolecules* **2020**, *53*, 3110–3118.
- (65) Nasir, A.; Yasin, T.; Islam, A. Thermo-oxidative degradation behavior of recycled polypropylene. *J. Appl. Polym. Sci.* **2011**, *119*, 3315–3320.
- (66) Dugas, L. D.; Walker, W. D.; Shankar, R.; Hoppmeyer, K. S.; Thornell, T. L.; Morgan, S. E.; Storey, R. F.; Patton, D. L.; Simon, Y. C. Diketamine-Based Vitrimers via Thiol-ene Photopolymerization. *Macromol. Rapid Commun.* **2022**, 2200249, 2200249.
- (67) Wang, T. X.; Chen, H. M.; Salvekar, A. V.; Lim, J.; Chen, Y.; Xiao, R.; Huang, W. M. Vitrimer-Like Shape Memory Polymers: Characterization and Applications in Reshaping and Manufacturing. *Polymer* **2020**, *12*, 2330.
- (68) Zhao, Q.; Zou, W.; Luo, Y.; Xie, T. Shape memory polymer network with thermally distinct elasticity and plasticity. *Sci. Adv.* **2016**, *2*, No. e1501297.



CAS BIOFINDER DISCOVERY PLATFORM™

STOP DIGGING THROUGH DATA —START MAKING DISCOVERIES

CAS BioFinder helps you find the
right biological insights in seconds

Start your search

CAS
A Division of the
American Chemical Society